PAPER

Check for updates

A novel molecular synthesis route to Li$_2$S loaded carbon fibers for lithium–sulfur batteries

Veronika Brune, [ID] [a] Christoph Bohr,[a] Tim Ludwig, [ID] [a] Michael Wilhelm,[a] Sebastian Daniel Hirt, [ID] [b] Thomas Fischer, [ID] [a] Sebastian Wennig,[b] Bernd Oberschachtsiek,[b] Arun Ichangi[a] and Sanjay Mathur [ID] *[a]

The synthesis of a novel air-stable molecular precursor (LiSC$_2$H$_4$)$_2$NMe enables the formation of the desired 1D lithium sulfide (Li$_2$S) *via* the electrospinning method under ambient conditions. The solubility of the precursor in polar solvents combined with a common polymer (PVP) allowed a suitable spinning solution to obtain ideal green Li$_2$S loaded fibers. 3D fiber mats of the calcined homogeneous 1D electrospun Li$_2$S/C fibers were characterized by electron microscopy and X-ray powder diffraction analysis. Direct integration of Li$_2$S in an electronically conductive carbon matrix as the cathode obviates the need of elemental lithium as the anode, which is a great advantage against the reported lithium–sulfur batteries. An initial capacity of about 870 mA h g^{-1} at C/20, a capacity retention of 73% after 100 cycles at C/10 and a capacity of about 400 mA h g^{-1} at 1C were observed for the presented system.

Introduction

The global rapid consumption of fossil fuels is directly linked to huge CO$_2$ emissions. Therefore, energy obtained from renewable sources like wind and solar is crucial for a sustainable energy supply.[1,2]

In this context, large-scale energy storage will play a key role in future energy technologies.[3] In general, batteries as electrochemical storage devices for different applications should meet several requirements of safety, high energy and power density, fast charging capability, sustainability and natural abundance of raw materials.[1] Among the innumerable energy-storage technologies, the lithium–sulfur battery has emerged as a promising alternative because of its high theoretical gravimetric energy density (about 2600 W h kg^{-1}).[4] Furthermore, sulfur is highly abundant, economically priced and non-toxic.[5–7] However, the low electrical conductivity of sulfur and lithium sulfide leads to limited high rate capability.[8] Additionally, the polysulfide shuttle effect and the volume change of about 80% during cell operation are further challenges of this battery system that have prevented its commercialization so far.[9–11] The volume change leads to mechanical stress within the cathode, which can result in electrode cracking and electrode pulverization as well.[12] The shuttle effect involves the dissolution of higher-ordered polysulfides (Li$_2$S$_4$–Li$_2$S$_8$) in the electrolyte, their migration to the anode, and their electrochemical reduction on

the anode's surface, which result in the formation of an additional passive layer composed of solid lithium sulfides such as Li$_2$S and Li$_2$S$_2$. This leads to an increased cell resistance. Lower-ordered lithium polysulfides diffuse back to the cathode, provoking chemical reactions with the cathode resulting in a decreased coulombic efficiency.[10] Finally, the shuttle effect causes a loss of the active material at the cathode, resulting in capacity fading.[13,14]

Applying elemental sulfur as the cathode material requires the deployment of elemental lithium as the anode. Lithium anodes can cause serious safety concerns since lithium dendrites can grow through the separator leading to short-circuits which can result in a thermal runaway.[15]

Recently, lithium sulfide (Li$_2$S) has received much attention as an electrochemically active cathode material in lithium–sulfur batteries because a lithium-free anode can be used and thus a higher level of safety can be ensured.[15] Li$_2$S also has a higher melting point than elemental sulfur, enabling the synthesis of advanced materials at higher temperatures. Therefore, Li$_2$S establishes various strategies for composite formation and surface modification to enhance the electrical conductivity of the cathode. A common method for achieving this purpose is the embedding of the active material in a carbon matrix.[16,17]

The synthesis of hierarchically porous 1D structures by electrospinning methods reveals an alternative synthetic approach to embed the active material in a flexible, free-standing, and conductive carbon matrix to accelerate the electronic and ionic transfer of the active material for improving the cycling stability.[18] This synthesis enables the formation of 1D-fibers with varying diameters owing to the influence of

[a]Institute of Inorganic Chemistry, University of Cologne, Greinstraße 6, D-50939 Cologne, Germany. E-mail: sanjay.mathur@uni-koeln.de
[b]The Fuel Cell Research Center, ZBT Duisburg, Carl-Benz-Straße 201, D-47057 Duisburg, Germany

changing process parameters such as the viscosity of spinning solution, voltage or kind of collector among others.[19–21] Porous carbon nanofibers tend to be an ideal matrix due to their low weight, high electronic conductivity and adjustable structural properties, meaning pore volume, pore size and specific surface area.[16,22,23] Furthermore, carbon fibers can mitigate polysulfide dissolution by enhanced chemical adsorption of intermediate species and therefore reduce the shuttle effect significantly.[19,24–27] A simple synthetic access to lithium sulfide cathodes is hampered by the moisture sensitivity and reactivity of lithium.[28] So far, the electrospinning of Li_2S has been limited to inert electrospinning devices or the use of Li_2SO_4 as the precursor, which can be reduced to Li_2S by a carbon source and hydrogen, respectively.[29,30] Li_2SO_4 has the advantages of non-inert handling due to its high stability against oxygen and moisture. As a drawback, the solubility of Li_2SO_4 is almost exclusive to aqueous solutions, which is a limiting factor in the choice of polymer for the electrospinning process.

By using different precursors instead of Li_2SO_4, Ye *et al.* achieved Li_2S/C fibers with high mass loading (72 wt%) by electrospinning a Li_2S_3/PVP precursor solution under inert conditions. The disadvantage of this synthesis route is that this precursor and material must be always under inert conditions, compared to our here presented molecular precursor.[31]

Using synthesized compounds to combine lithium and sulfur already at a molecular level shows the advantages of preformed Li–S bonds and the opportunity to shield and protect the sensitive Li–S unit against oxidation by introducing a suitable ligand. Therefore, we combined the dianionic, tridentate SNS ligand system $((HSC_2H_4)_2NMe)$ with a suitable lithium source (butyllithium). The stabilizing properties and clear thermal decomposition of this ligand system have already been reported in molecular precursor synthesis before.[32]

To overcome the current limitations in the synthesis of Li_2S electrospun fibers, a molecular approach towards a stable synthesized precursor will be presented in the following, which, to the best of our knowledge, has not been reported before. This molecular precursor enables the electrospinning of lithium sulfide-based fibers under ambient conditions from a single precursor solution, which is not limited to only aqueous solutions, ensuring a simple preparation of Li_2S/C nanofibers. The scheme in Fig. 1 shows the battery configuration with Li_2S loaded fibers as the cathode material, which have been provided by a novel synthetic approach, and will be described within this work.

Results & discussion

Complexes of the tridentate ligand *N*-methyldiethanethiol-amine (**I**) with lithium-delivered molecular precursors of formula $(LiSC_2H_4)_2NMe$ were successfully synthesized and characterized. The *N*-methyldiethanethiolamine was synthesized according to a process described in the literature before (Scheme 1a) and isolated by distillation under reduced pressure as a colorless oil.[32–34] To deprotonate the thiol function of the isolated compound **I**, an acid–base reaction of *n*-butyllithium or lithium alcoholate was performed in *n*-heptane to produce the lithium derivative *N*-methyldiethanethiolatoamine-lithium $(LiSC_2H_4)_2NMe$ (**I-Li**) (Scheme 1b) as a colorless solid. The synthesized compound is air-stable and soluble in protic solvents such as alcohols or water as well as in dimethylsulfoxide (DMSO). The appropriate solubility combined with good stability reveals that the compound is an ideal precursor for a simple preparation of lithium sulfide materials.[14,35,36] The comfortable handling under ambient conditions and high degrees of freedom regarding the choice of solvents make this molecular compound an ideal precursor for material processing methods.

The new compound was analyzed by multi-nuclear magnetic resonance (NMR) spectroscopy using a combination of 1D and 2D NMR experiments (^1H, ^{13}C, $^1H^1H$ COSY, $^1H^{13}C$ HSQC, $^1H^{13}C$ HMBC). For **I**, three different proton signals were detected with an integrative ratio of 2 : 3 : 8 (Fig. 2b) which is attributed to the symmetry of **I** along with the methyl function and the nitrogen, showing the possible free rotation around the CH_2 axis.
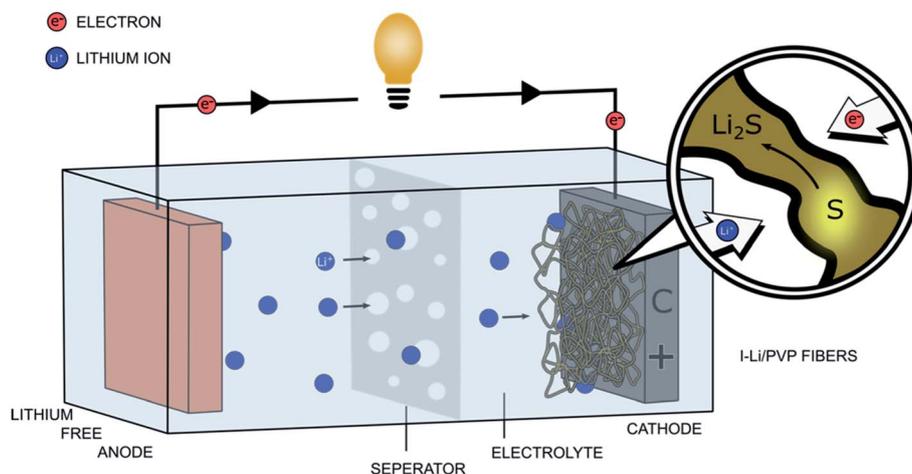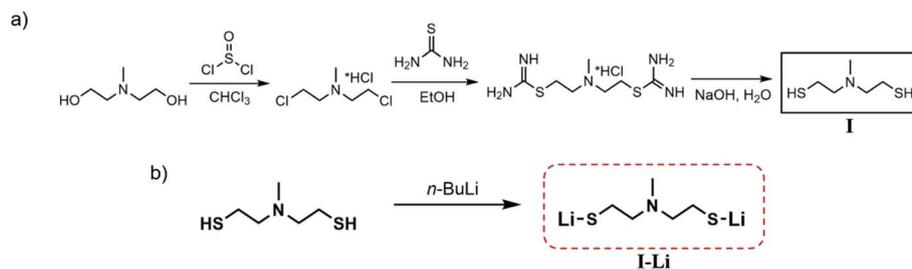

Fig. 1 Illustration of the battery configuration with **I-Li**/PVP fibers as the cathode material in a lithium free anode.

This journal is © The Royal Society of Chemistry 2022

J. Mater. Chem. A, 2022, **10**, 9902–9910 | **9903**

Scheme 1 (a) General synthesis route to N-methyldiethanethiolamine (HSC$_2$H$_4$)$_2$NMe (**I**) modified from ref. 32 and (b) synthesis of N-methyl-diethanethiolatoamine-lithium (LiSC$_2$H$_4$)$_2$NMe (**I-Li**).
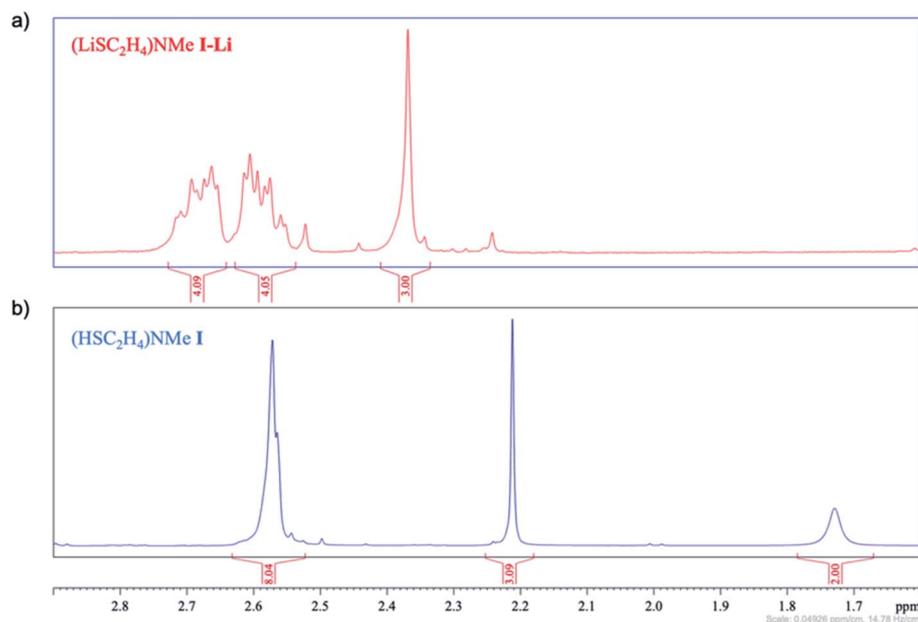
Fig. 2 ^{1}H NMR of (a) (LiSC$_2$H$_4$)$_2$NMe **I-Li** and (b) (HSC$_2$H$_4$)$_2$NMe **I**.

The signals of both ethanethiol chains appear as one signal with an equal chemical shift located at 2.58 ppm. The two acidic thiol protons resulted in a broad signal at 1.74 ppm and the methyl group was found at 2.24 ppm. The NMR spectroscopic studies of compound **I** were in agreement with the literature[34] and corroborated the proposed structure of the ligand in solution (Fig. 2b). The deprotonation of **I** by treatment with butyl-lithium resulted in the lithium derivative **I-Li** (Fig. 2a) showing separated CH$_2$ protons for the ethanethiol chains in NMR analysis, resulting from the hindered rotation around the C–C-axis. In total 11 protons were detected, confirming the depro-tonation of pre-synthesized ligand **I** and successful proton exchange by the desired alkali metal.

To investigate the thermal decomposition behavior of **I-Li**, thermogravimetric measurements were performed under an inert atmosphere (Fig. 3a). The multi-step decomposition showed a total weight loss of 72% at temperatures up to 800 °C, resulting in the formation of crystalline residue of lithium sulfide (Li$_2$S). The decomposition of molecular precursor sets in at around 100 °C and a nearly complete decomposition was observed at around 350 °C. At this point, Li$_2$S was already

formed in an amorphous phase, which was confirmed by XRD measurements.[37,38] At elevated temperatures, beginning at 650 °C, conversion to the crystalline cubic phase of Li$_2$S takes place.

X-ray diffraction investigations of the decomposition residue obtained at 800 °C under a nitrogen atmosphere confirmed the formation of the desired crystalline Li$_2$S phase (Fig. 3b). The simple thermal decomposition to phase pure Li$_2$S in combina-tion with the comfortable operation, good solubility in protic solutions and air stability qualified the synthesized precursor **I-Li** as an efficient molecular source for the fabrication of Li$_2$S loaded carbon-based 1D materials.

Therefore, (LiSC$_2$H$_4$)$_2$NMe–PVP aligned fiber mats were produced from ethanolic solutions of **I-Li** with poly-vinylpyrrolidone (PVP) by the electrospinning process (Fig. 4).

Calcination of electrospun fibers was performed by applying a ramping of 2 °C min^{-1} up to 280 °C (holding time 2 h) under ambient conditions, to stabilize the fibrous structure by partly oxidizing,[39] followed by a temperature increase of 2 °C min^{-1} up to 700 °C (holding time 5 h) under a nitrogen atmosphere to finalize the carbonization process and to produce crystalline
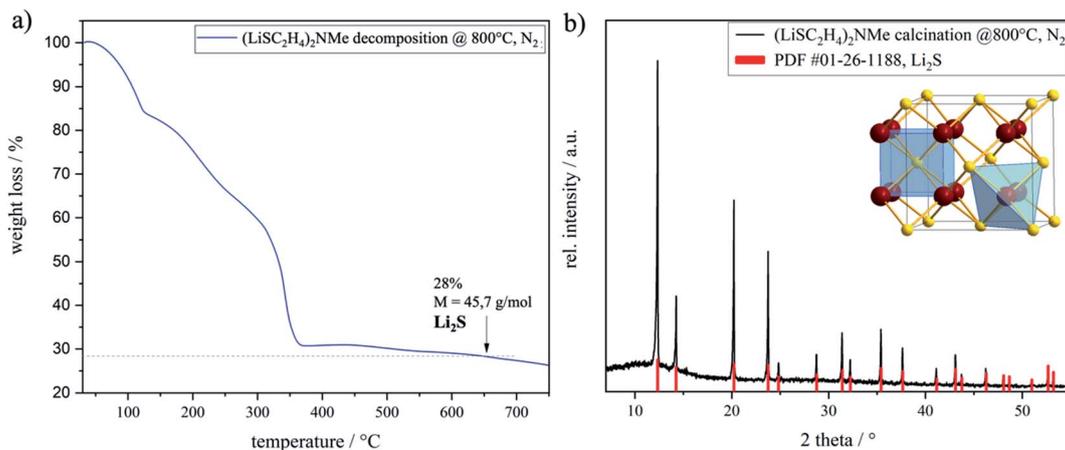
9904 | J. Mater. Chem. A, 2022, **10**, 9902–9910

This journal is © The Royal Society of Chemistry 2022

Fig. 3   (a) Thermogravimetric measurements of the synthesized precursor (LiSC$_2$H$_4$)$_2$NMe I-Li up to 800 °C under a nitrogen atmosphere; (b) XRD pattern of the decomposed compound I-Li to the corresponding lithium sulfide Li$_2$S (ref. PDF #01-26-1188).
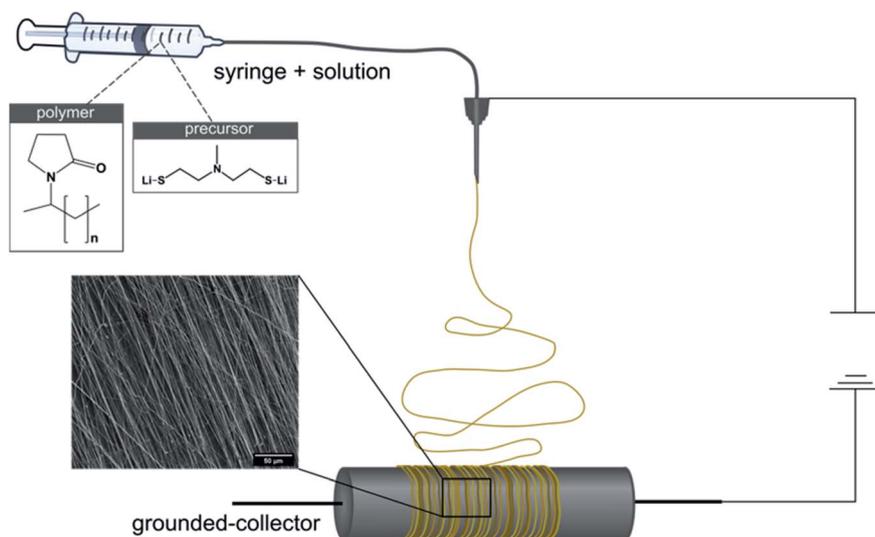

Fig. 4   Electrospinning of the I-Li/PVP solution with a drum collector.

Li$_2$S/C-fiber mats (I-Li/C_45%, Fig. 5a), respectively. The desired product formation was confirmed by XRD measurements of the calcined specimen (Fig. 5b).

A precursor solution with an I-Li to PVP ratio of 1 : 1.5 was used to yield an appropriate viscosity for electrospinning which is mandatory to produce homogeneous fibers. A rotary drum
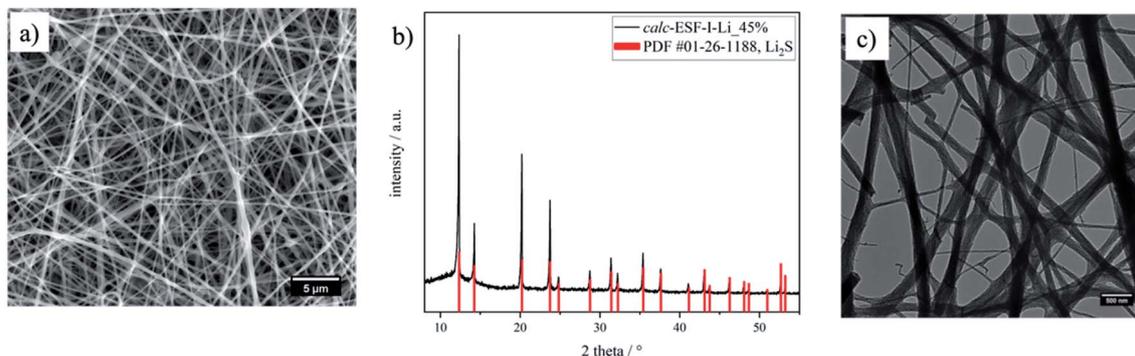

Fig. 5   Electrospun I-Li fibers containing 45% Li$_2$S in their calcined form. (a) SEM image of the electrospun green I-Li fibers (I-Li/PVP_58%), (b) XRD of I-Li/C_45% (ref. PDF #01-26-1188) and (c) TEM image of the calcined electrospun I-Li fibers (I-Li/C_45%).

collector was chosen since electrospinning onto a stationary collector led to low fiber adhesion towards the aluminum foil with bundling or aggregation effects. The aligned composite fiber (**I-Li**/PVP_58%) contained a (LiSC$_2$H$_4$)$_2$NMe mass fraction of 58 wt%. After the calcination process, a lithium sulfide/conductive carbon composite fiber mat with a total Li$_2$S fraction of 45 wt% (**I-Li**/C_45%) was obtained which was determined by thermogravimetric measurements.

TEM analysis of **I-Li**/C_45% displayed a 3D fiber network out of 1D electrospun fibers (Fig. 5c).[39] The porosity of the fiber structure leads to a high surface-to-volume ratio and therefore to an intensive contact between the active material and electrolyte, which results in fast lithium-ion diffusion enabling higher charge and discharge rates.

Electrodes made from **I-Li**/C_45% fibers, PVP as the binder and carbon black as the conductive additive were characterized electrochemically.

Cyclic voltammetry (Fig. 6a) was used to investigate the electrochemical behavior of **I-Li**/C_45% fibers. In the first cycle, two oxidation peaks located at 2740 mV *vs.* Li/Li$^+$ and at 3710 mV *vs.* Li/Li$^+$ were observed. In the literature, the first peak at 2751 mV *vs.* Li/Li$^+$ is attributed to side reactions or the formation of sulfur from Li$_2$S or polysulfides.[40,41] The broad peak between 3170 and 3900 mV *vs.* Li/Li$^+$ with a maximum at 3708 mV *vs.* Li/Li$^+$ is assigned to the oxidation of Li$_2$S to lithium

polysulfides and sulfur, respectively. Usually, the oxidation of Li$_2$S to elemental sulfur is located between 2200 and 2600 mV *vs.* Li/Li$^+$ depending on particle size and active material loading.[42,43] The size of the crystalline Li$_2$S material was calculated using Scherrer's equation at around 10 nm. However, for the activation of a fresh Li$_2$S cathode, a higher potential within the first cycle is required.[44] The overpotential was necessary for phase nucleation of polysulfides, the removal of surface passivation[44] and successive further oxidation to elemental sulfur.[43] This phenomenon has been reported for electrodes containing PVP, due to the interaction of lithium ions from Li$_2$S with the oxygen functions of the PVP matrix.[45] A significant current flow was still observed between 3900 and 4000 mV *vs.* Li/Li$^+$, which can be assigned to side reactions such as electrolyte decomposition. For the oxidation reaction, a capacity of 1456 mA h g^{-1} was calculated from the CV. This capacity is 290 mA h g^{-1} higher than the theoretical capacity of Li$_2$S. Presumably, this can be explained by side reactions such as electrolyte decomposition and the shuttle mechanism, respectively. Three cathodic peaks located at 2355, 2111 and 2025 mV *vs.* Li/Li$^+$ were observed, which were assigned to the reduction of sulfur. At 2355 mV *vs.* Li/Li$^+$ the reaction of elemental sulfur (S$_8$ ring) with two lithium ions forming long-chain polysulfide Li$_2$S$_8$ has been observed.[42] The reduction peak at 2111 mV *vs.* Li/Li$^+$ is not characteristic for all Li$_2$S cathodes. However, it can be
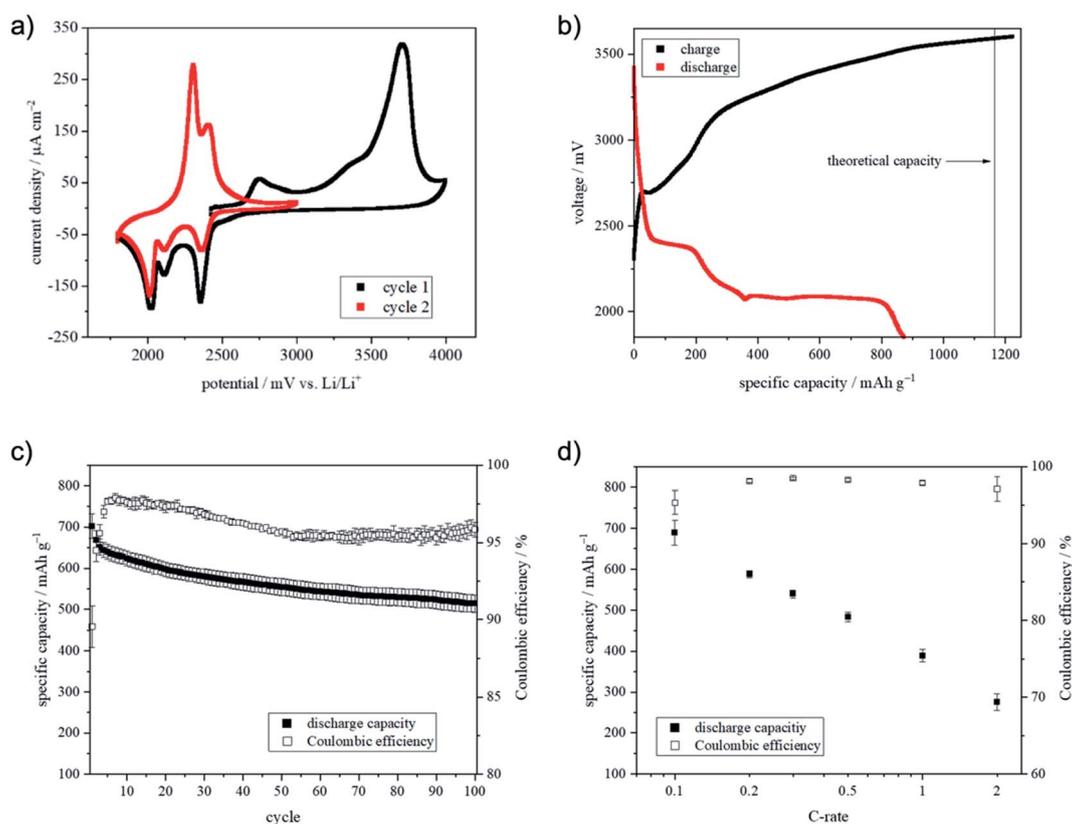

Fig. 6 (a) Cyclic voltammogram of **I-Li**/C_45%; (b) voltage profile of the first cycle measured at C/20; (c) specific capacity retention of **I-Li**/C_45% at C/10 when cycled between 2600 and 1850 mV and (d) discharge capacities and coulombic efficiencies of **I-Li**/C_45% at different C-rates; each data point represents the mean value of five cycles at the specific current from three different cells.

9906 | *J. Mater. Chem. A*, 2022, **10**, 9902–9910

This journal is © The Royal Society of Chemistry 2022

assigned to the further reduction of the long-chained Li_2S_8 to the shorter-chained polysulfide Li_2S_4.[46] The electrochemical conversion of Li_2S_4 to Li_2S_2 and Li_2S occurred at 2025 mV vs. Li/Li$^+$. The calculated capacity for the reduction was 863 mA h g^{-1} giving a coulombic efficiency of 59.2%. A low coulombic efficiency in the first cycle was already described in the literature and can be explained by the formation of passivation layers as well as by the dissolution of polysulfides in the electrolyte.[47] For the second cycle, the cut-off oxidation potential was set to 3000 mV vs. Li/Li$^+$. Two anodic peaks at 2307 and 2407 mV vs. Li/Li$^+$ were detected. The peak at 2307 mV vs. Li/Li$^+$ corresponded to the formation of short-chain polysulfides and the latter peak was assigned to the formation of long-chain polysulfides and sulfur, respectively.[48,49] The 1705 mV vs. Li/Li$^+$ lower oxidation potential of the second cycle was identified as a common phenomenon of Li_2S cathodes.[50] The polysulfides, which were formed in the first cycle, dissolved in the electrolyte and catalyzed the oxidation of Li_2S to S_8 leading to a lower oxidation potential.[51]

The reductive peaks showed comparable potentials as identified in the first cycle, which was consistent with the literature.[52–54] Additionally, cycling experiments were performed to evaluate the capacity, capacity retention and high-rate capability (Fig. 6b–d).

The initial cycle was performed at C/20 and the voltage profile is shown in Fig. 6b.

During the charging process, a small plateau at 2696 mV was observed, which seemed to be corresponding to the peak at 2740 mV vs. Li/Li$^+$ in the first cycle of the CV. The voltage shift resulted from the cell setup (CV: three-electrode configurations, cycling: two-electrode configuration) as well as the different current flow. As seen in Fig. 6a the cell voltage rose after the plateau drastically. However, the voltage seemed to run into a plateau at about 3600 mV instead of reaching the set cut-off voltage of 3900 mV. This leads to the presumption that the polysulfide shuttle had a strong influence on cell voltage. The shuttle caused a constant voltage by generating polysulfides which were reduced and re-oxidized at the electrode.[55] Additionally, electrolyte decomposition at a voltage higher than 3500 mV vs. Li/Li$^+$ was more and more likely. Hence, the charging process was stopped after 21 h.

The further cycles were recorded at C/10 (Fig. 6c).

A capacity of 702 mA h g^{-1} and capacity retention of 73% after 100 cycles were observed. The mean coulombic efficiency was 96%. The reason for the limited coulombic efficiency could be the side reactions caused by the polysulfide shuttle.[56] In comparison with the Li_2S–C–PVP material of Liu et al.[45] the material showed a slightly lower initial capacity. However, after 50 cycles the capacity of Liu's material reached 460 mA h g^{-1} instead of the 554 mA h g^{-1} for **I-Li**/C_45%.[45] Perhaps, this can be explained by the better structural integrity of our material.

Additionally, the high-rate capability was measured by applying different currents (Fig. 6d). A reduced capacity at higher C-rates is a commonly known property of lithium–sulfur batteries[57] and can be explained by the slow kinetics of the polysulfide redox reaction and the very low electrical conductivity of the lithium–sulfur species.[58] The presented material

Table 1 Concentrations of spinning solutions

Sample ID	Precursor concentration [mol L^{-1}]	PVP concentration [mol L^{-1}]
I-Li/PVP_58%	0.46	4.29×10^{-5}

showed at a rate of 1C at least 56% of the capacity at 0.1C. This promising result can be explained by the good electrical connection between the particles and of the particles with the current collector, respectively.

Conclusion

Herein, we demonstrated a novel molecular approach to lithium sulfide for battery application. Characterization of the synthesized molecular precursor ($LiSC_2H_4$)$_2$NMe) provides an extraordinary control of the desired material formation. Good solubility in various solvents enables simple handling and an innovative preoperational fabrication carbon embedded Li_2S. Ethanolic solution of both compounds, polymer and precursor, united in the same spinning solution makes the preparation of a suitable electrospinning system possible, which resulted in homogeneous Li_2S/C-based fiber mats. Calcination of the electrospun fibers provides Li_2S loaded fiber mats, which in the case of Li_2S/C show a capacity retention of 73% over 100 cycles and a capacity of about 400 mA h g^{-1} at 1C. For further application of electrospun Li_2S loaded carbon fibers the usage of PVP with lower molecular weight will allow higher Li_2S loading through optimized PVP/**I-Li** ratios in the spinning solution. This will have influence on the electrochemical performance of battery cells.

The use of the as-prepared molecular precursor and the application of the so obtained Li_2S/C as the cathode material enable lithium metal free lithium–sulfur batteries with a higher safety level.

Introducing heavier alkali metals to the discussed molecular precursor system shows first promising results for the synthesis of ($M^I SC_2H_4$)$_2$NMe (M^I = Na, K) compounds and from that the preparation of Na_2S and K_2S materials, which is still under investigation.

Experimental

All manipulations of air- and moisture-sensitive materials were carried out under a nitrogen atmosphere using stock-type all-glass assemblies. All solvents and reactants were used without further purification, except otherwise mentioned. n-Butyl lithium (2.5 M in n-hexane solution) and polyvinylpyrrolidone (PVP, 1 300 000 g mol^{-1}) were purchased from Acros Organics. NMR spectra were recorded on a Bruker Avance II 300 spectrometer; chemical shifts are quoted in parts per million relative to external TMS (^{1}H and ^{13}C). Thermal analysis was performed on a TGA/DSC 1 (Mettler-Toledo GmbH, Germany) in a nitrogen atmosphere (25 mL min^{-1}) at a rate of 10 °C min^{-1} from 30 to 800 °C. For the determination of the Li_2S amount in the final product, synthetic air was used at a rate of 10 °C min^{-1} from 30

This journal is © The Royal Society of Chemistry 2022

J. Mater. Chem. A, 2022, **10**, 9902–9910 | **9907**

to 800 °C. This temperature was held for 5 h. The sample weight was in the range of 5–20 mg. Room temperature powder X-ray diffraction (XRPD) was conducted on an STOE-STADI MP diffractometer, operating in transmission mode using Mo Kα (λ = 0.71073 Å) radiation. Measured peak patterns were compared to reference powder diffraction files (PDF). The crystallite size of the produced Li_2S in electrospun fibers was calculated from the line broadening analysis of the most intense diffraction peak using Scherrer's equation; $D\frac{1}{4}K\lambda/(\beta \cos \theta)$, where D is the coherently diffracting domain size (average crystallite size), K is the shape factor (0.94), λ is the wavelength of the X-ray radiation, β is the full width at half maximum (FWHM) measured in radians and θ is the Bragg angle. The size and morphology of the obtained fibers were analyzed using an FEI Strata Dual Beam 235 focused ion beam coupled scanning electron microscope (FIB-SEM) and a JEOL JEM-2200FS transmission electron microscope (TEM). A FuG electronics GmbH high voltage power supply and a Landgraf Laborsysteme LA-100 syringe pump were used for electrospinning. As spinnerets, 21G (inner diameter 0.5 mm) blunt needles were applied. The synthesis of $(HSC_2H_4)_2$-NMe **I** has been described before.[32]

Synthesis of *N*-methyl-diethanethiolamine-lithium $(LiSC_2H_4)_2NMe$ (I-Li)

12.60 mL (31.20 mmol) of 2.5 M *n*-butyl lithium in *n*-hexane were added to a liquid nitrogen-cooled solution of *N*-methyl-diethanethiolamine (2.39 g, 15.60 mmol) in 10 mL heptane and stirred for 30 min at room temperature. The resulting colorless powder was washed several times with *n*-heptane. Afterward, the solvent was removed under reduced pressure. The product was isolated as a colorless solid in a yield of 94% (2.39 g, 14.60 mmol).

^{1}*H NMR (D_2O, 300 MHz, RT, ppm): 2.37 (s, 3H, –NCH_3), 2.61 (m, 4H, –NCH_2CH_2S–), 2.66 (m, 4H, –SCH_2CH_2N–).*

^{13}*C NMR (D_2O, 75 MHz, RT, ppm): 20.4 (–SCH_2CH_2N–), 40.4 (–NCH_3), 62.4 (–SCH_2CH_2N–).*

Preparation of the composite metal sulfide/conductive carbon fiber mats

In a typical electrospinning process, the corresponding spinning solution (see Table 1) was fed with a feed rate of 10 μL min^{-1}. The distance between the needle and rotary drum collector was kept constant at 15 cm and a high voltage of 15 kV was applied. The process was conducted at room temperature with relative humidity below 35%.

The obtained green fibers were calcined in a tubular furnace with a temperature program of 1 °C min^{-1} up to 280 °C (holding for 2 h) under ambient conditions, followed by a temperature increase of 1 °C min^{-1} up to 700 °C (holding for 3 h) under a nitrogen atmosphere. All handling after calcination was performed under strictly inert conditions.

Electrode preparation and electrochemical testing

Cathode preparation and assembly of test cells were done in an argon-filled glovebox (MBraun, Germany). The contents of oxygen and moisture were below 2.0 ppm. First, the synthesized active material (**I-Li**/C_45%) was homogenized and mixed with carbon black (Super P C65, Timcal) using a mortar. PVP (PVP K90, AppliChem) was dissolved in *N*-methyl-2-pyrrolidone (NMP, Acros Organics) to form a binder solution. Afterward, the mixture of active material and carbon black was added to the binder solution. The suspension was homogenized by magnetic stirring to form a slurry. The ratio of the active material, carbon black and PVP was set to 80 : 5 : 15. The corresponding slurry was cast on a non-woven carbon (Sigracet 28AA, SGL Carbon SE) using a doctor blade. Subsequently, the electrodes were dried at 90 °C under vacuum for 16 hours. Finally, the electrodes with a diameter of 13 mm (coin cells) and 12 mm (Swagelok® T-cells) were punched out. The loading of Li_2S was about 0.5 mg cm^{-2}.

A solution of 1.0 M lithium bis(trifluoromethane sulfonyl) imide (LiTFSI, Sigma Aldrich) and 0.2 M lithium nitrate ($LiNO_3$, Alfa Aesar) in 1,3-dioxolane (DOL, Sigma Aldrich) and dimethoxyethane (DME, Sigma Aldrich) (1 : 1, v/v) served as the electrolyte for the electrochemical investigation.

The charge/discharge experiments of the Li_2S electrodes were performed in coin cells (CR 2032, Hohsen Corp.) with a BasyTec CTS-Lab XXL. Lithium metal (Alfa Aesar, thickness: 380 μm) served as the counter electrode. A glass fiber filter (GF/ D, Whatman) soaked with 100 μl electrolyte was used as the separator. The formation of the cells was done at 0.05C between 3900 and 1850 mV. Further cycles were recorded between 2600 and 1850 mV by applying various currents which correspond to C rates between C/10 and 2C. The charge/discharge measurements were carried out as triple determination, and the average values of capacities are shown as representative results.

Cyclic voltammograms (CV) were recorded with a Gamry Interface 5000E potentiostat in Swagelok® T-cells using a three-electrode configuration. The CVs of Li_2S electrodes were recorded between 1800 and 4000 mV *vs.* Li/Li$^+$ (initial cycle) and between 1800 and 3000 mV *vs.* Li/Li$^+$ (second cycle), respectively, at a scan rate of 50 μV s^{-1}. Lithium metal was used as the counter and reference electrode and polypropylene fleeces (FS2190, Freudenberg) soaked with electrolyte 300 μl were used as the separator.

Author contributions

9908 | *J. Mater. Chem. A*, 2022, **10**, 9902–9910

This journal is © The Royal Society of Chemistry 2022

Conflicts of interest

There are no conflicts to declare.

Acknowledgements

References

1 X. Fan, J. Yue, F. Han, J. Chen, T. Deng, X. Zhou, S. Hou and C. Wang, *ACS Nano*, 2018, **12**, 3360–3368.

2 B. Dunn, H. Kamath and J. M. Tarascon, *Science*, 2011, **334**, 928–935.

3 R. C. Longo, L. E. Camacho-Forero and P. B. Balbuena, *J. Chem. Phys.*, 2020, **152**, 014701.

4 P. G. Bruce, S. A. Freunberger, L. J. Hardwick and J. M. Tarascon, *Nat. Mater.*, 2012, **11**, 19–29.

5 Y. Xiao, S. H. Lee and Y. K. Sun, *Adv. Energy Mater.*, 2017, **7**, 1601329.

6 C. Van Pham, L. Liu, B. Britton, M. Walter, S. Holdcroft and S. Thiele, *Sustainable Energy Fuels*, 2020, **4**, 1180–1190.

7 J. Yan, W. Li, R. Wang, P. Feng, M. Jiang, J. Han, S. Cao, Z. Zhang, K. Wang and K. Jiang, *ACS Energy Lett.*, 2020, **5**, 1307–1315.

8 J. Huo and Y. Wang, *Int. J. Electrochem. Sci.*, 2020, **15**, 1529–1538.

9 X. Fang and H. Peng, *Small*, 2015, **11**, 1488–1511.

10 S. F. Ng, M. Y. L. Lau and W. J. Ong, *Adv. Mater.*, 2021, **2008654**, 1–54.

11 Y. C. Ho and S. H. Chung, *Chem. Eng. J.*, 2021, **422**, 130363.

12 A. Manthiram, Y. Fu, S. H. Chung, C. Zu and Y. S. Su, *Chem. Rev.*, 2014, **114**, 11751–11787.

13 Z. Sun, M. Xiao, S. Wang, D. Han and S. Song, *J. Mater. Chem. A*, 2014, **2**, 9280–9286.

14 X. Zhang, H. Xie, C. S. Kim, K. Zaghib, A. Mauger and C. M. Julien, *Mater. Sci. Eng., R*, 2017, **121**, 1–29.

15 D. Su, D. Zhou, C. Wang and G. Wang, *Adv. Funct. Mater.*, 2018, **28**, 1–23.

16 J. Liu, Z. Li, B. Jia, J. Zhu, W. Zhu, J. Li, H. Pan, B. Zheng, L. Chen, G. Pezzotti, *et al.*, *J. Mater. Chem. A*, 2020, **8**, 6303–6310.

17 Z. Tong, L. Huang, W. Lei, H. Zhang and S. Zhang, *J. Energy Chem.*, 2021, **54**, 254–273.

18 X. Ge, S. Liu, M. Qiao, Y. Du, Y. Li, J. Bao and X. Zhou, *Angew. Chem., Int. Ed.*, 2019, **58**, 14578–14583.

19 T. Pakki, E. H. Mohan, N. Y. Hebalkar, J. Adduru, S. V. Bulusu, A. Srinivasan, K. M. Mantravadi and N. R. Tata, *J. Mater. Sci.*, 2019, **54**, 9075–9087.

20 S. Cavaliere, S. Subianto, I. Savych, D. J. Jones and J. Rozière, *Energy Environ. Sci.*, 2011, **4**, 4761–4785.

21 G. Sun, L. Sun, H. Xie and J. Liu, *Nanomaterials*, 2016, **6**, 1–30.

22 C. H. Chang, S. H. Chung and A. Manthiram, *Mater. Horiz.*, 2017, **4**, 249–258.

23 P. Strubel, S. Thieme, T. Biemelt, A. Helmer, M. Oschatz, J. Brückner, H. Althues and S. Kaskel, *Adv. Funct. Mater.*, 2015, **25**, 287–297.

24 W. Ren, W. Ma, X. Jin, S. Zhang and B. Tang, *ChemSusChem*, 2019, **12**, 2447–2456.

25 Q. Cheng, W. Xu, S. Qin, S. Das, T. Jin, A. Li, A. C. Li, B. Qie, P. Yao, H. Zhai, *et al.*, *Angew. Chem., Int. Ed.*, 2019, **58**, 5557–5561.

26 D. Liu, C. Zhang, G. Zhou, W. Lv, G. Ling, L. Zhi and Q. H. Yang, *Adv. Sci.*, 2018, **5**, 1700270.

27 M. Liu, N. Deng, J. Ju, L. Fan, L. Wang, Z. Li, H. Zhao, G. Yang, W. Kang, J. Yan, *et al.*, *Adv. Funct. Mater.*, 2019, **29**, 1–34.

28 K. Han, J. Shen, C. M. Hayner, H. Ye, M. C. Kung and H. H. Kung, *J. Power Sources*, 2014, **251**, 331–337.

29 M. Yu, Z. Wang, Y. Wang, Y. Dong and J. Qiu, *Adv. Energy Mater.*, 2017, **7**, 1700018.

30 Z. Li, S. Zhang, C. Zhang, K. Ueno, T. Yasuda, R. Tatara, K. Dokko and M. Watanabe, *Nanoscale*, 2015, **7**, 14385–14392.

31 F. Ye, Y. Hou, M. Liu, W. Li, X. Yang, Y. Qiu, L. Zhou, H. Li, Y. Xu and Y. Zhang, *Nanoscale*, 2015, **7**, 9472–9476.

32 V. Brune, C. Hegemann and S. Mathur, *Inorg. Chem.*, 2019, **58**, 9922–9934.

33 J. Harley-Mason, *J. Chem. Soc.*, 1947, **74**, 320–322.

34 M. Sun, C. Hong and C. Pan, *J. Am. Chem. Soc.*, 2012, 20581–20584.

35 A. Fotouhi, D. Auger, L. O'Neill, T. Cleaver and S. Walus, *Energies*, 2017, **10**, 1937.

36 K. Patel, *J. Undergrad. Res.*, 2016, **9**, 39–42.

37 X. Meng, D. J. Comstock, T. T. Fister and J. W. Elam, *ACS Nano*, 2014, **8**, 10963–10972.

38 F. Ye, M. Liu, X. Yan, J. Li, Z. Pan, H. Li and Y. Zhang, *Small*, 2018, **14**, 1–7.

39 J. W. Jung, C. L. Lee, S. Yu and I. D. Kim, *J. Mater. Chem. A*, 2016, **4**, 703–750.

40 M. Yu, Z. Wang, Y. Wang, Y. Dong and J. Qiu, *Adv. Energy Mater.*, 2017, **7**, 1700018.

41 X. Chen, L. Peng, L. Yuan, R. Zeng, J. Xiang, W. Chen, K. Yuan, J. Chen, Y. Huang and J. Xie, *J. Energy Chem.*, 2019, **37**, 111–116.

42 X. Huang, Z. Wang, R. Knibbe, B. Luo, S. A. Ahad, D. Sun and L. Wang, *Energy Technol.*, 2019, **7**, 1801001.

43 Y. Yang, G. Zheng, S. Misra, J. Nelson, M. F. Toney and Y. Cui, *J. Am. Chem. Soc.*, 2012, **134**, 15387–15394.

44 Y. Jung and B. Kang, *Phys. Chem. Chem. Phys.*, 2016, **18**, 21500–21507.

45 J. Liu, H. Nara, T. Yokoshima, T. Momma and T. Osaka, *J. Power Sources*, 2015, **273**, 1136–1141.

46 K. Cai, M.-K. Song, E. J. Cairns and Y. Zhang, *Nano Lett.*, 2012, **12**, 6474–6479.

47 Z. W. Seh, J. H. Yu, W. Li, P.-C. Hsu, H. Wang, Y. Sun, H. Yao, Q. Zhang and Y. Cui, *Nat. Commun.*, 2014, **5**, 5017.

48 B.-J. Lee, H.-Y. Park, D.-S. Yang, T.-H. Kang, S. Hwang and J.-S. Yu, *J. Electrochem. Soc.*, 2019, **166**, A5244–A5251.

This journal is © The Royal Society of Chemistry 2022

J. Mater. Chem. A, 2022, **10**, 9902–9910 | **9909**

49 Y. Fu and A. Manthiram, *J. Phys. Chem. C*, 2012, **116**, 8910–8915.

50 Y. Yang, G. Zheng, S. Misra, J. Nelson, M. F. Toney and Y. Cui, *J. Am. Chem. Soc.*, 2012, **134**, 15387–15394.

51 Y. Fu, Y. S. Su and A. Manthiram, *Adv. Energy Mater.*, 2014, **4**, 1–5.

52 K. Cai, M.-K. Song, E. J. Cairns and Y. Zhang, *Nano Lett.*, 2012, **12**, 6474–6479.

53 M. Yu, Z. Wang, Y. Wang, Y. Dong and J. Qiu, *Adv. Energy Mater.*, 2017, **7**, 1700018.

54 Y. Chen, S. Lu, J. Zhou, W. Qin and X. Wu, *Adv. Funct. Mater.*, 2017, **27**, 1700987.

55 Y. Diao, K. Xie, S. Xiong and X. Hong, *J. Power Sources*, 2013, **235**, 181–186.

56 M. Wild, L. O'Neill, T. Zhang, R. Purkayastha, G. Minton, M. Marinescu and G. J. Offer, *Energy Environ. Sci.*, 2015, **8**, 3477–3494.

57 T. Zhang, M. Marinescu, S. Walus, P. Kovacik and G. J. Offer, *J. Electrochem. Soc.*, 2018, **165**, A6001–A6004.

58 Y. Tao, Y. Wei, Y. Liu, J. Wang, W. Qiao, L. Ling and D. Long, *Energy Environ. Sci.*, 2016, **9**, 3230–3239.

9910 | *J. Mater. Chem. A*, 2022, **10**, 9902–9910

This journal is © The Royal Society of Chemistry 2022